Table 1 Reaction of hydrocarbons with nitric acid

Hydrocarbon	O/F volume ratio = 1:1		O/F volume ratio = 2:1		O/F volume ratio = 4:1	
	Pressure at 2 msec, psi	Maximum pressure, psi	Pressure at 2 msec, psi	Maximum pressure, psi	Pressure at 2 msec, psi	Maximum pressure, psi
n-pentane	...	...	...	...	...	...
n-hexane[a]	10,110	37,680	...	...	...	...
n-heptane	16,030 ± 3,980	27,520 ± 2,126	17,600 ± 2,000	32,700 ± 3,100	14,600 ± 3,300	29,000 ± 4,440
n-octane	19,150 ± 1,160	30,730 ± 2,840	20,200 ± 900	36,400 ± 1,400	13,600 ± 3,300	26,800 ± 3,500
n-decane[b]	23,000 ± 3,080	33,750 ± 1,150	17,100 ± 200	29,200 ± 1,700	13,820 ± 3,500	29,900 ± 3,200
n-dodecane	...	...	7,500 ± 1,700	24,600 ± 1,400	10,200 ± 2,400	24,200 ± 2,700
n-hexadecane	...	...	6,600 ± 3,200	21,800 ± 7,500	8,700 ± 4,700	27,600 ± 3,300

[a] Out of many attempts only one ignition was obtained.
[b] The burning rate of decane was sometimes lower than reported here, corresponding more to the values shown for dodecane and hexadecane. On any given day the results were the same, but they varied from day to day, presumably because of the poor ambient temperature control in the laboratory. This phenomenon was not observed with the other fuels.

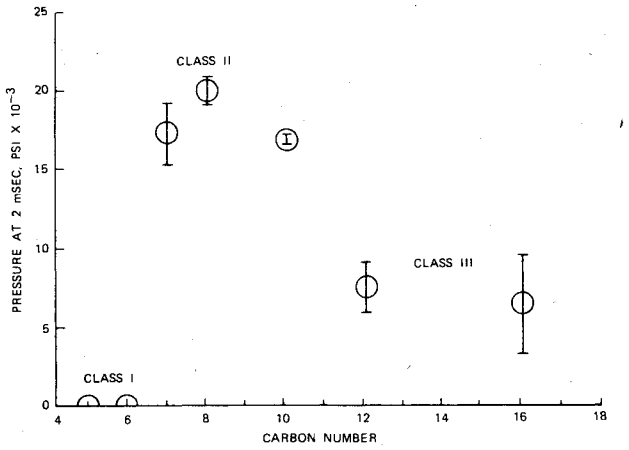

Fig. 4 Effect of carbon number on pressurization rate for n-alkane/nitric acid combustion/O/F volume ratio = 2:1).

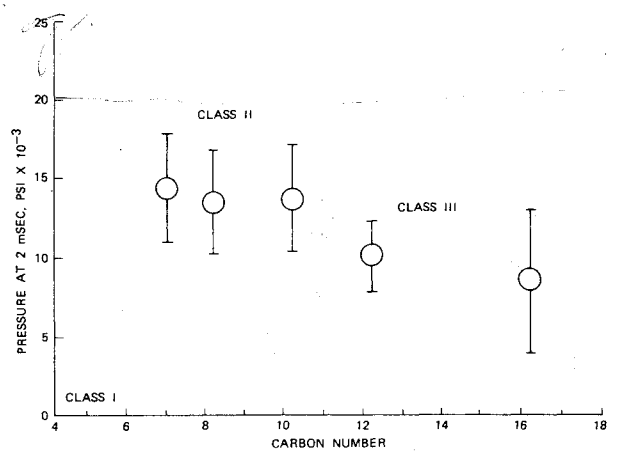

Fig. 5 Effect of carbon number on pressurization rate for n-alkane/nitric acid combustion /O/F volume ratio = 4:1).

pact-pressure pulse is used as a measure of the pressurization rate; the maximum pressure reached in 18 msec (total sweep time of the scope) is also tabulated.

Figures 3-5 are pressure (at 2 msec) vs carbon number plots for the three O/F ratios tested. All the data points in Table 1 and Figs. 3-5 represent the mean of at least three measurements except the point for hexane at a volume O/F ratio of 1:1; hexane reacted only once out of many attempts. It appears that the n-alkanes can be divided into three categories of reactivity: 1) *Class I:* high-volatility fuels (pentane, hexane) which are unreactive because they present an overly fuel-rich vapor phase in combination with 90% nitric acid. 2) *Class II:* intermediate-volatility fuels (heptane, octane) which produce a combustible vapor phase prior to, or shortly after, impact and are very reactive. 3) *Class III:* low-volatility fuels which require a significant fraction of the impact energy for vaporization to produce a combustible vapor mixture and are slowly reactive.

Vapor pressure calculations reveal that the room-temperature gas-phase acid/hydrocarbon composition is closest to stoichiometric for n-nonane. Lower and higher alkanes give fuel-rich and oxidizer-rich vapor mixtures, respectively; thus the vapor-composition explanation of the relative reaction rates of the n-alkanes is consistent with the data.

Summary and Conclusions

A Technoproducts Olin-Mathieson drop-weight tester pressure cell has been applied to the study of the ignition and high-pressure (up to 36,000 psi) combustion of a two-phase, nonhypergolic bipropellant combination, 90% nitric acid and n-alkanes. The results indicate optimum combustion for C_7 to C_{10} alkanes. Higher and lower alkanes burned more slowly and less reproducibly and were harder to ignite.

References

[1] "Liquid Propellant Test Methods," Chemical Propulsion Information Agency, Silver Spring, Md., 1960.

[2] Griffin, D.N., "Initiation of Liquid Propellants and Explosives by Impact," American Rocket Society Technical Paper 1706-61, Palm Beach, Fla., 1961.

Hemisphere-Cylinder in Transonic Flow, $M_\infty = 0.7 \sim 1.0$

Tsuying Hsieh*
Arnold Engineering Development Center, Arnold Air Force Station, Tenn.

Nomenclature

a = local sound speed
c_p = pressure coefficient

Received April 16, 1975; revision received May 27, 1975. The research reported herein was conducted by the Arnold Engineering Development Center, Air Force Systems Command. Research results were obtained by personnel of ARO, Inc., Contract Operator of AEDC. Further reproduction is authorized to satisfy needs of the U.S. Government.

Index categories: Subsonic and Transonic Flow; Jets, Wakes, and Viscid-Inviscid Flow Interactions.

*Research Engineer, PWT/4T. Member AIAA.

K = curvature of the body in the meridian plane
M = Mach number
n, s = body-oriented coordinate system
p = pressure
R = radius of the cylinder
r, Z = radial and axial distances, respectively
u, v = velocity components in the n and s directions, respectively
θ = inclination angle of the body
κ = $1+Kn$
ϕ = velocity potential
∞ = freestream condition

Introduction

THE application of a hemisphere-cylinder as a flow probe or sensing device shape is well known. However, few theoretical or experimental studies have been reported about a hemisphere-cylinder in transonic, supercritical flow. One of the reasons has perhaps been the lack of an effective theoretical method to compute the flowfield, even when the fluid is assumed to be inviscid, until the publication of Ref. 1. Another factor may have been the complicated flowfield caused by the interaction of boundary-layer separation and the embedded normal shock, as reported in a great number of papers in the study of transonic airfoils. As a first step in understanding the flowfield of a hemisphere-cylinder in transonic, super-critical flow, experimental and theoretical studies of the flowfield were carried out for freestream Mach numbers, M_∞ from 0.7 to 1.0. A similar study, conducted for M_∞ from 1.05 to 2.0, has been published separately.[2]

Experimental Investigation

Experiments were performed for the purpose of understanding the flow phenomena and comparing these experimental results with inviscid theoretical prediction, which are described later. A 1-in.-diam and 10-in.-long hemisphere-cylinder was sting-mounted in the AEDC 1-ft-square, continuous, transonic wind tunnel. A description of the wind tunnel is given in Ref. 3. Pressure data were taken for M_∞ from 0.7 to 1.0 and shadowgraphs were taken for $M_\infty = 0.8$, 0.9, 0.95, and 1.0. The unit Reynolds numbers in this experiment varied from 4.6 ($M_\infty = 0.7$) to 5.3 x 10^6 ($M_\infty = 1.0$) with variation in static pressure of 2050 psf to 1480 psf and temperature of 134°F to 132.6°F, respectively.

Theoretical Investigation

In the theoretical investigation, the relaxation solution of the steady, full potential equation given by South and Jameson[1] is utilized to predict the inviscid flowfield. The differential equation solved is as follows:

$$\left(1-\frac{u^2}{a^2}\right)\frac{1}{\kappa}\left(\frac{\partial\phi}{\partial s}\left(\frac{1}{\kappa}\frac{\partial\phi}{\partial s}\right)\right) - 2\frac{uv}{\kappa a^2}\frac{\partial^2\phi}{\partial s\partial n} + \left(1-\frac{v^2}{a^2}\right)\frac{\partial^2\phi}{\partial n^2} + \left[\frac{K}{\kappa}\left(1-\frac{u^2}{a^2}\right)+\frac{\cos\theta}{r}\right]\frac{\partial\phi}{\partial n} + \left[2\frac{Kuv}{\kappa a^2}+\frac{\sin\theta}{r}\right]\frac{1}{\kappa}\frac{\partial\phi}{\partial s} = 0 \tag{1}$$

The relations between ϕ and the velocity components are

$$u = \cos\theta + (1/\kappa)(\partial\phi/\partial s) \tag{2a}$$

$$v = \sin\theta + (\partial\phi/\partial n) \tag{2b}$$

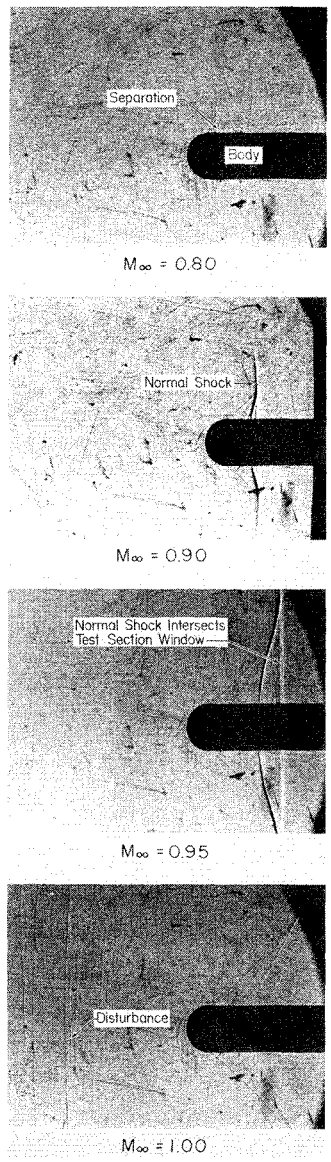

Fig. 1 Shadowgraphs of flow past hemisphere-cylinder.

Along the axis, Eq. (1) reduces to its limiting form

$$\frac{2}{\kappa^2}\frac{\partial^2\phi}{\partial s^2} + \left(1-\frac{v^2}{a^2}\right)\frac{\partial^2\phi}{\partial n^2} + 2\frac{K}{\kappa}\frac{\partial\phi}{\partial n} = 0 \tag{3}$$

The boundary conditions to be satisfied are

$$\phi \to 0 \text{ as } n \to \infty \tag{4a}$$

$$v = 0 \text{ or } \partial\phi/\partial n = \sin\theta \text{ on the body surface} \tag{4b}$$

As described in Ref. 1, sheared cylindrical coordinates are used for the afterbody. For the hemisphere-cylinder, Eqs. (1-4) remain the same for the sheared cylindrical coordinates. In performing calculations, one locates infinity about one body length beyond the body and station.

Results and Discussion

In Fig. 1, the shadowgraphs of flow past a hemisphere-cylinder are shown for $M_\infty = 0.8$, 0.9, 0.95, and 1.0. As seen in the shadowgraph for $M_\infty = 0.8$, a clear boundary-layer separation starts in the vicinity of the tiny normal shock. As M_∞ increases, the normal shock grows and moves downstream; at the same time the separation is reduced. A com-

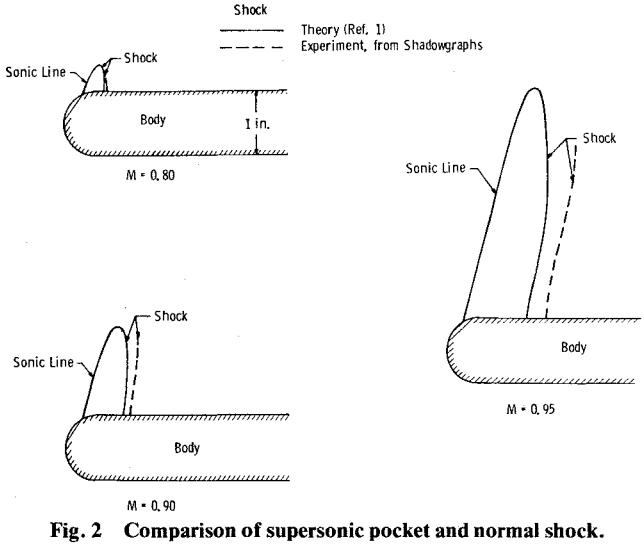

Fig. 2 Comparison of supersonic pocket and normal shock.

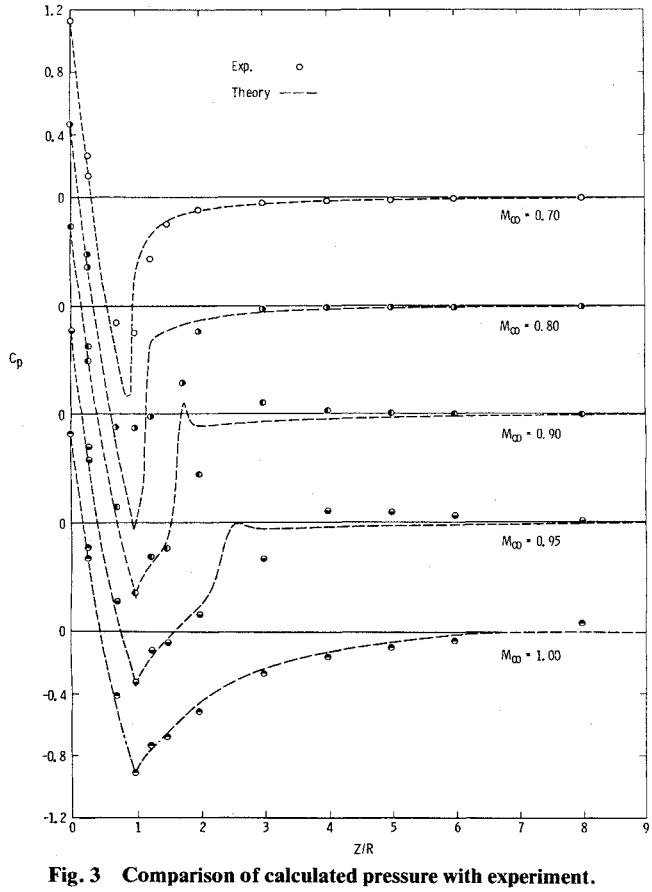

Fig. 3 Comparison of calculated pressure with experiment.

parison of the location of the supersonic pocket and shock calculated by the relaxation method and obtained from the shadowgraphs of Fig. 1 is presented in Fig. 2. The shape of the shock is predicted correctly, but the location of the shock obtained experimentally is shifted some distance downstream.

The surface pressure calculated by the relaxation method is compared with the experimental data for M_∞ from 0.7 to 1.0 in Fig. 3. The theory predicts the pressure distribution correctly from the nosetip until the point at which the shock seems to appear. For $M_\infty = 0.8$ there is significant disagreement between the theoretical and experimental pressure distributions. The corresponding shadowgraph given in Fig. 2 does indicate a pronounced boundary-layer separation; therefore, the inviscid theory fails to work there. For $M_\infty = 1$, it is surprising to see the good agreement between the predicted and measured surface pressure.

In conclusion, from experimental and theoretical results it is shown that an interaction of boundary-layer separation and shock waves strongly influences the flow over a hemisphere-cylinder in the transonic Mach number range; therefore, the inviscid theory fails to predict the flow. Such interaction is particularly strong when $M_\infty \sim 0.8$. Further study, both theoretical and experimental, is required to have a better understanding of the flow.

References

[1] South J. Jr. and Jameson, A. "Relaxation Solutions for Inviscid Axisymmetric Transonic Flow over Blunt or Pointed Bodies," *Proceedings, of the AIAA Computational Fluid Dynamic Conference*, July 1973.

[2] Hsieh, T. "Flowfield Study about a Hemispherical Cylinder in Transonic and Low Supersonic Mach Number Range," AIAA Paper 75-83, Washington, D.C., 1975.

[3] Jackson, F.N. and Sloan, E.H. "Calibration of the AEDC-PWT 1-Foot Transonic Tunnel." AEDC-TR-68-4 (AD827912), Feb. 1968, Arnold Engineering Development Center, Arnold Air Force Base, Tenn.

Fuel Atomization in a Flowing Airstream

K. V. L. Rao*
National Aeronautical Laboratory, Bangalore, India

and

A. H. Lefebvre†
Cranfield Institute of Technology, Cranfield, Bedford, England

Nomenclature

SMD = mean drop size, microns (10^{-6}m)
V = air velocity, m/sec
ΔP = fuel injection pressure, N/m^2
FN = atomizer flow number (liters/hr)/(N × m^2)$^{0.5}$
R = volume fraction of spray composed of drops larger than d
d = drop diameter, μ
$\bar{d}$ = drop size parameter, μ
x = drop size distribution parameter

Introduction

WHEN a swirl atomizer is used to inject fuel into a flowing airstream the resultant mean drop size represents the combined effects of a) the initial atomization produced by the swirl atomizer, plus b) the secondary atomization arising from the airblast action of the flowing airstream. In conventional gas turbine combustion chambers the primary-zone velocity is usually too low to have any discernible influence on atomization quality. However, in duct burners of the type employed in some modern turbofan engines, and in the "premix-prevaporization" systems designed for low-emission combustors, the air velocity may be so high as to affect appreciably the mean drop size of the spray. Under these conditions calculations of fuel evaporation

Received, March 17, 1975; revision received May 23, 1975.
Index categories: Airbreathing Propulsion, Subsonic and Supersonic; Combustion in Heterogeneous Media.

*Scientist, Propulsion Division.

†Professor and Head of the School of Mechanical Engineering.